



Article

# Cucurbit[*n*]uril (*n* = 6, 7) Based Carbon-Gold Hybrids with Peroxidase-Like Activity

Liangfeng Zhang, Yan Zeng, Simin Liu and Feng Liang \*

The State Key Laboratory of Refractories and Metallurgy, Coal Conversion and New Carbon Materials Hubei Key Laboratory, School of Chemistry & Chemical Engineering, Wuhan University of Science and Technology, Wuhan 430081, China; wustzlf@163.com (L.Z.); zengyan@wust.edu.cn (Y.Z.); liusimin@wust.edu.cn (S.L.)

\* Correspondence: feng\_liang@whu.edu.cn; Tel.: +86-027-6886-2107

Received: 4 April 2018; Accepted: 20 April 2018; Published: 24 April 2018



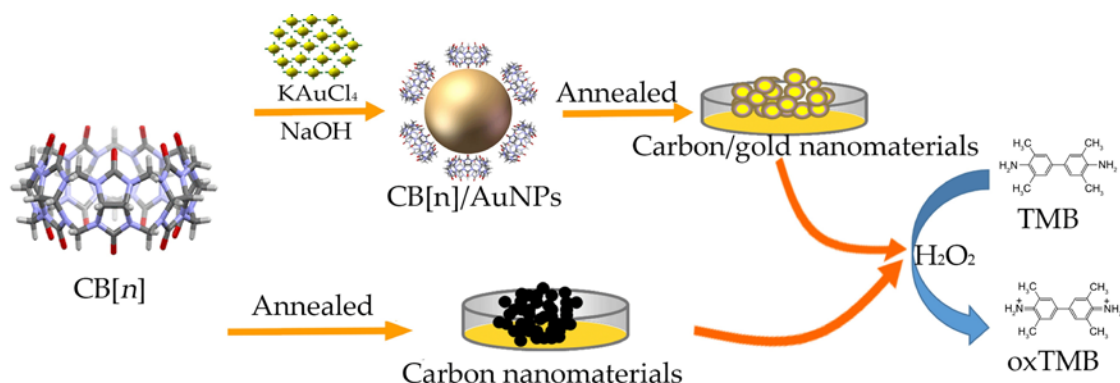
**Abstract:** Despite the combination of molecular recognition and local electric field enhancement endowing cucurbit[*n*]uril-capped metallic nanoparticles, indicating great potential in a variety of areas, prior work has paid little attention to carbonizing cucurbit[*n*]uril on the surface of gold nanoparticles, which may propose new carbon-gold hybrid materials with interesting applications. In this work, we developed a simple and cost-effective method to prepare carbon-gold hybrids by carbonizing cucurbit[*n*]uril modified gold nanoparticles. The as-prepared cucurbit[*n*]uril based carbon and carbon-gold hybrid materials have shown to possess peroxidase-like activity. All cucurbit[*n*]uril based nanomaterials exhibited high catalytic activity over a pH range 2–6 and more tolerant to high temperature (up to 60 °C) when compared to natural horseradish peroxidase.

**Keywords:** cucurbit[*n*]uril; gold nanoparticles; carbon-gold hybrid; peroxidase-like activity

## 1. Introduction

The cucurbit[*n*]uril (CB[*n*]) family, which bears a rigid hydrophobic cavity and two identical carbonyl fringed portals, is one of the most important macrocyclic containers in host-guest chemistry. The carbonyl oxygen atoms of the cucurbit[*n*]uril can coordinate directly to a variety of metal ions and lead to complicated nanoscale frameworks and architectures [1]. Since Li and colleagues unraveled the direct interactions between surface of gold nanoparticles and the electron-rich carbonyl rims of CB[*n*] for the first time [2], CB[*n*] has been commonly used in capping gold and other metallic nanoparticles with applications, such as in catalysis, drug delivery, electrochemical analysis and surface-enhanced Raman spectroscopy (SERS) [3,4]. In spite of this, there are very few reports of carbonization of CB[*n*] on the surface of gold nanoparticles, which may be expected to bring new carbon-gold hybrid materials with interesting applications. Previous studies have shown that carbon-gold nanocomposites have excellent biocompatibility, electric conductivity, and physical and chemical stability [5–10].

The long-term goal of our group is to construct carbon, metal and carbon-metal hybrid nanomaterials for emerging catalytic, sensing and biological applications [11–17]. In our previous work, we developed carbon nanomaterials decorated with metal nanoparticles by ion implantation and chemical deposition [18–20], in which the metal particles adhered poorly to the carbon material. Recently, we developed a sonication and solvothermal method to prepare carbon nanomaterials [21–23] that can degrade hydrogen peroxide to produce hydroxyl radicals, and thus possess intrinsic peroxidase-like activity [22]. Herein, we demonstrate a simple and cost-effective method to prepare carbon-gold hybrids by carbonizing cucurbit[*n*]uril modified gold nanoparticles, as illustrated in Scheme 1. The prepared materials exhibited high catalytic activity over a pH range 2~6 and were more tolerant to high temperature when compared to natural horseradish peroxidase (HRP).



**Scheme 1.** Schematic illustration of preparation of cucurbit[*n*]uril based carbon-gold and carbon nanomaterials with peroxidase-like activity.

## 2. Materials and Methods

### 2.1. Chemicals

Sodium hydroxide, hydrogen peroxide, disodium hydrogen phosphate dodecahydrate, sodium chloride and 3,3',5,5'-tetramethylbenzidine (TMB) were purchased from Sinopharm Chemical Reagent Co., Ltd. (Shanghai, China). Horseradish peroxidase was purchased from Hubei Xinxin Belle Biotechnology Co., Ltd. (Wuhan, China). Potassium tetrachloroaurate (III) was purchased from Sahn Chemical Technology Co., Ltd. (Shanghai, China). Cucurbit[6]uril and cucurbit[7]uril were synthesized by our group [14,17].

### 2.2. Cucurbit[*n*]uril Directed Synthesis of Gold Nanoparticles (AuNPs)

The aqueous solution of CB[6] (5 mmol, 25 mL) and CB[7] (5 mmol, 25 mL) was prepared with the assistance of sodium chloride (29 mg) because CB[6] partially dissolved in double distilled water. After that, one equivalent amount of aqueous KAuCl<sub>4</sub> (5 mmol, 25 mL) was mixed with CB[6] or CB[7] solution at room temperature. A yellow precipitate was immediately obtained, then an aqueous solution of NaOH (40 mmol, 50 mL) was added. The yellow precipitate disappeared, and a clear solution was obtained; then, a wine-red colored solution formed after 48 h, indicating the formation of the AuNPs.

### 2.3. Preparation of Cucurbit[*n*]uril Based Carbon-Gold and Carbon Nanomaterials

Initially, the resulting wine red AuNPs was washed three times with double distilled water by means of centrifugation. After that, AuNPs solution was sealed in Teflon-lined stainless-steel autoclave (100 mL) and reacted at 180 °C for 24 h by using Vacuum oven DZF-6020 (Shanghai Jinghong, Shanghai, China). After the autoclave was cooled down to the room temperature, the pre-carbonized materials were collected by means of centrifugation. The obtained khaki powder was dried in vacuum at 40 °C, then carbonized in quartz crucible up to 700 °C under a nitrogen atmosphere at a heating rate of 5 °C/min, and then held at that temperature for 1 h by using a vacuum tube furnace, OTF-1200X. Carbon nanomaterials were directly prepared from CB[6] and CB[7] in a quartz crucible by heating up to 700 °C under a nitrogen atmosphere at a rate of 5 °C/min, and then held at that temperature for 1 h.

### 2.4. Materials Characterization

The UV-vis absorption spectra were recorded on Shimadzu UV-vis-NIR spectrophotometer (Shimadzu, Tokyo, Japan). Transmission electron microscopy (TEM) was performed by using JEM-2100UHR STEM (JEOL, Tokyo, Japan). Energy-dispersive X-ray spectroscopy (EDS) measurements were performed with a spectrometer attached to PHILIPS XL30 TMP field-emission scanning electron microscopy (SEM) system

(Philips, Hillsboro, OR, USA). The X-ray powder diffraction (XRD) pattern was tested on a X'Pert PRO MPD diffractometer (Panalytical B.V., Amsterdam, Holland) with nickel-filtered Cu  $K_{\alpha}$  radiation. A thermal gravimetric analyzer (TGA) STA449 (Nai Chi Scientific Instruments, Shanghai, China) was used for the investigation of the thermal properties of the samples.

### 2.5. Peroxidase-Like Activity

To investigate the peroxidase-like activity of carbon-gold and carbon nanomaterials, catalytic oxidation of the colorimetric substrate TMB in the presence of  $H_2O_2$  was performed. In a typical experiment [22], the mixture of TMB (8 mM, 100  $\mu$ L), carbon-gold (40  $\mu$ L) or carbon nanomaterials (1 mg/mL), phosphate buffer (25 mM, 810  $\mu$ L, pH = 4), together with  $H_2O_2$  (1 M, 50  $\mu$ L) are incubated at 35  $^{\circ}$ C for standard curve measurement. Under the above-mentioned condition, the catalytic reaction was incubated in the buffer solution under different pH (1.0–12.0) to investigate the pH effect on the tested reaction. Similarly, the reaction was incubated in the buffer solution under different temperature from 25  $^{\circ}$ C to 60  $^{\circ}$ C to examine the effect of temperature. HRP was investigated under the same conditions as the control.

Under optimum conditions, the steady-state kinetic parameters of carbon-gold ( $C_{CB[n]}/AuNPs$ ) and carbon nanomaterials ( $C_{CB[n]}$ ) as catalysts were determined by using  $H_2O_2$  and TMB as substrates. In the presence of  $H_2O_2$  and TMB, the reaction was carried out at 35  $^{\circ}$ C in a 1 mL of a tube containing prepared nanomaterials or HRP in phosphate buffer solution (25 mM, pH = 4). The assays were carried out by varying concentration of TMB at a fixed concentration of  $H_2O_2$  or varying concentration of  $H_2O_2$  at a fixed concentration of TMB. The reaction kinetics measurements were performed by recording the absorbance reading at 652nm in the time scan mode.

## 3. Results and Discussion

### 3.1. Characterization of Prepared Nanomaterials

As illustrated in Scheme 1,  $KAuCl_4$  in  $CB[n]$  solution produced  $CB[n]$  capped AuNPs under a specific set of conditions [24–27]. The  $CB[n]$  plays the role of both reducing and protecting agents. The particles obtained were spherical in shape and had good dispersibility as shown in Figure 1. UV-vis spectroscopy of AuNPs are shown in Figure 1a, the characteristic surface plasmon resonance band of these two kinds of AuNPs centered at 547 nm and 540 nm, respectively. The size of AuNPs was investigated by transmission electron microscopy (TEM), as shown in Figure 1b,c, and the mean diameter of the  $CB[n]$  capped AuNPs,  $CB[6]/AuNPs$  and  $CB[7]/AuNPs$  were  $8.0 \pm 1.5$  nm and  $10.0 \pm 1.1$  nm.

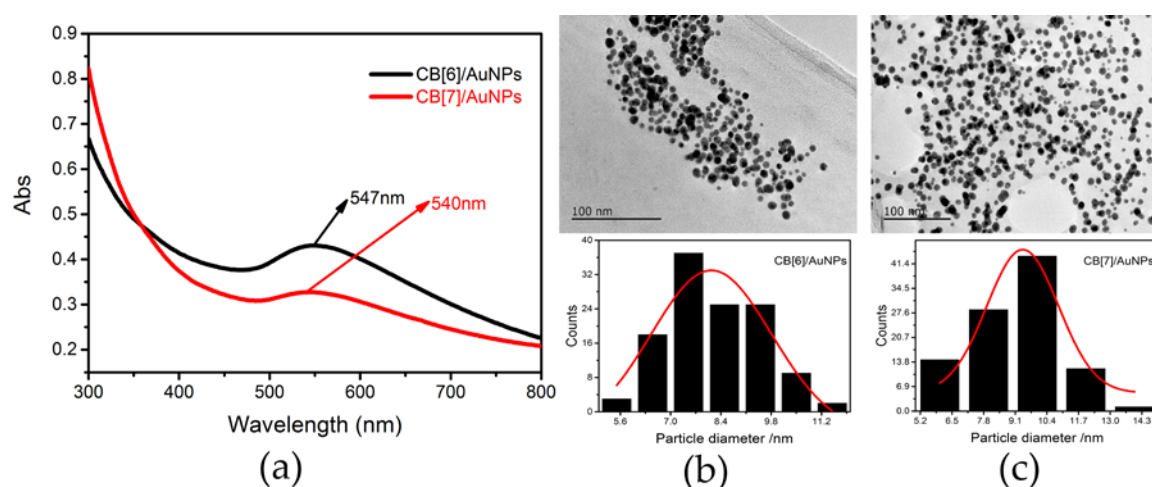


**Figure 1.** (a) UV-vis spectra of the prepared AuNPs. TEM micrographs and their corresponding histograms of (b)  $CB[6]/AuNPs$  and (c)  $CB[7]/AuNPs$ .

In order to confirm the morphology of the annealed CB[6]/AuNPs and CB[7]/AuNPs hybrid materials ( $C_{CB[6]}/AuNPs$  and  $C_{CB[7]}/AuNPs$ ), scanning electron microscopy (SEM) and transmission electron microscopy (TEM) were applied to study the prepared materials. The SEM images in Figure 2a,e show that these hybrid materials have three-dimensional porous structures. EDS spectroscopy was further used to confirm the hybrid nanomaterials. As shown in Figure 2b,f, EDS only detected gold and carbon in the composites, suggesting that these hybrids are composed of gold and carbon elements. Moreover, X-ray diffraction patterns were utilized to detect the crystal structures of two hybrids. The diffraction peaks observed from the blue line of Figure 2d,h at  $38.2^\circ$ ,  $44.4^\circ$ ,  $64.7^\circ$ ,  $77.7^\circ$  and  $81.8^\circ$  could be ascribed to the (111), (200), (220), (311) and (222) planes of the Au crystals, and a broad peak at  $20^\circ$ – $30^\circ$  related to the amorphous carbon of cucurbit[*n*]uril [28,29], which further confirms that the hybrid materials are composites of gold and carbon. In addition, the black strip of Au is embedded in the carbon film irregularly, as evidenced by the TEM images in Figure 2c,g.

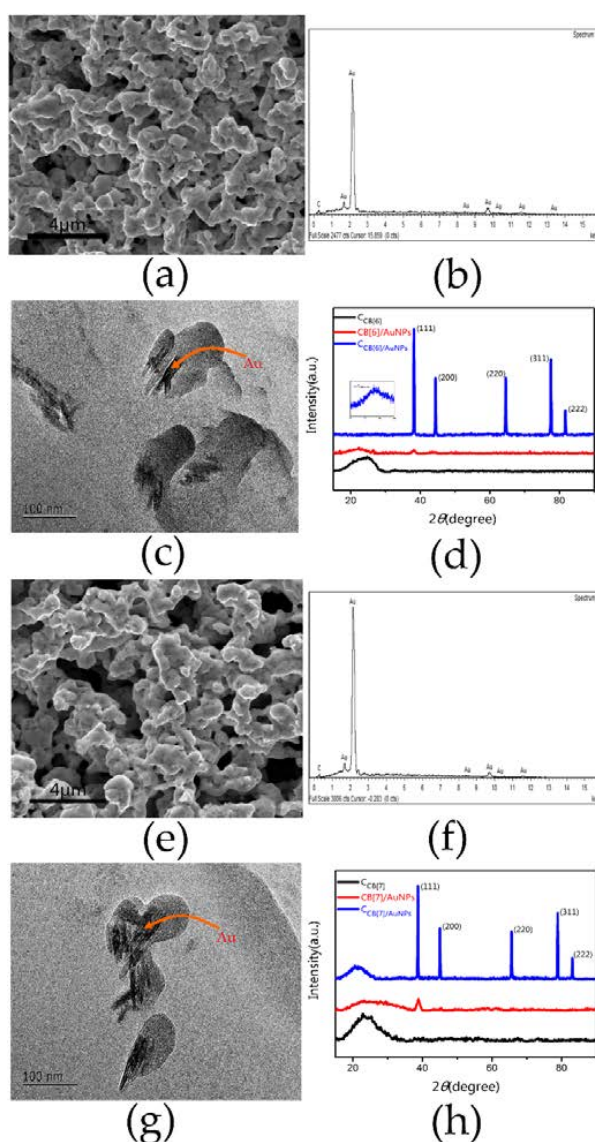


**Figure 2.** (a) Secondary electron SEM image of  $C_{CB[6]}/AuNPs$ ; (b) EDS pattern of  $C_{CB[6]}/AuNPs$ ; (c) TEM image of  $C_{CB[6]}/AuNPs$ ; (d) XRD pattern of CB[6] and corresponding materials; (e) Secondary electron SEM image of  $C_{CB[7]}/AuNPs$ ; (f) EDS pattern of  $C_{CB[7]}/AuNPs$ ; (g) TEM image of  $C_{CB[7]}/AuNPs$ ; (h) XRD pattern of CB[7] and corresponding materials.

Thermal gravimetric analysis (TGA) was used to investigate the weight loss of CB[6] and CB[7]. As shown in Figure 3, there are two steps to weight loss. The slight weight loss from the first stage could be attributed to the release of physically absorbed water, and the other loss is from the pyrogenation of cucurbit[n]urils [17]. The annealed cucurbit[7]uril ( $C_{CB[7]}$ ) is multilayer stacking of porous structures (the pore size is around  $0.56 \pm 0.13 \mu\text{m}$ ), while the annealed cucurbit[6]uril ( $C_{CB[6]}$ ) is the layer by layer stacking structure, with no obvious pores detected. The thickness of  $C_{CB[7]}$  sheet ( $1.47 \pm 0.29 \mu\text{m}$ ) is thicker than that of  $C_{CB[6]}$  ( $0.97 \pm 0.32 \mu\text{m}$ ).

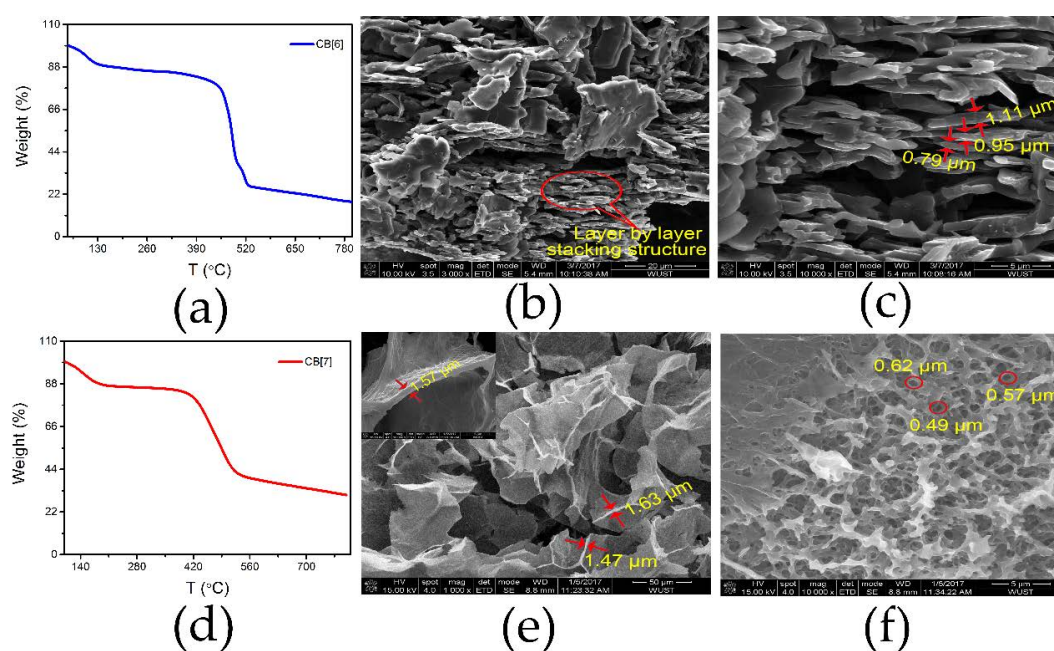


**Figure 3.** TGA curves of (a) CB[6] and (d) CB[7]; Secondary electron SEM images of  $C_{CB[6]}$ : (b,c); Secondary electron SEM images of  $C_{CB[7]}$ : (e,f).

### 3.2. Peroxidase-Like Activity

The catalytic performance of as-prepared carbon-gold and carbon nanomaterials were tested by using the peroxidase substrate TMB. Upon the addition of  $\text{H}_2\text{O}_2$ , the catalytic reaction can be monitored by detecting TMB absorbance change at 652 nm [22,30,31]. As shown in Figure 4, no obvious absorbance peak at 652 nm could be detected in the mixed solution of TMB and prepared materials of TMB and  $\text{H}_2\text{O}_2$ . After the addition of  $\text{H}_2\text{O}_2$ , the absorption peak at 652 nm was significantly enhanced in the presence of prepared nanomaterials over the same period. These results clearly demonstrated that prepared hybrids and carbon nanomaterials in this work possessed intrinsic peroxidase-like activity. As shown in Figure S1, with the increasing concentration of TMB, the absorbance at 652 nm changed quickly, suggesting that more TMB was oxidized. Furthermore, TMB can be detected by the prepared materials as low as  $1 \times 10^{-4} \text{ mol/L}$ , which is similar to HRP [32–35].

Similar to other peroxidase mimics as well as the natural peroxidase HRP, the catalytic activity of hybrids and carbon nanomaterials is also dependent on pH and temperature [32,33]. It is well known that pH is an important parameter for a catalytic reaction. The pH dependent experiments were performed in the buffer solution with different pH values range from 1.0 to 12.0. Similar to the natural peroxidase HRP, the optimal pH is 4. In addition, hybrids and carbon nanomaterials are much more stable over a relatively wide pH range. As shown in Figure 5a–d, when the pH of the buffer solution is 5, the peroxidase-like activity of hybrids and carbon nanomaterials remained 80%, while the HRP almost drifted to inactive performance. Moreover, the influence of temperature on the TMB oxidation reaction catalyzed by the as-prepared nanomaterials and HRP were investigated by varying the reaction temperature from 25 °C

to 60 °C, as illustrated in Figure 5e,f. Due to the sensitivity of HRP to temperature, the natural enzyme easily becomes denatured, while the catalytic activity of hybrids and carbon nanomaterials increased gradually with increasing experimental temperatures. However, the catalytic activity of hybrids and  $C_{CB[6]}$  dramatically decreased at a temperature higher than 55 °C, except for  $C_{CB[7]}$ , which continuously increased with the higher temperature. This might be attributed to the honeycomb-like porous structure and larger pore volume of  $C_{CB[7]}$  as shown in Figure 3. Although it has been reported that  $Fe_3O_4@C$  nanoparticles [33] and  $CeO_2$  nanoparticles [34] exhibited temperature-dependent catalytic activity, the exact mechanism underlying such activity is still unclear. The evolution of oxidation of TMB under  $H_2O_2$  as a function of pH and temperature was conducted. As shown in Figure S2,  $H_2O_2$  could be more efficient in oxidizing TMB at higher temperatures under acidic conditions. Increasing the temperature could accelerate the decomposition of  $H_2O_2$  to produce oxygen and benefit the oxidation of TMB.

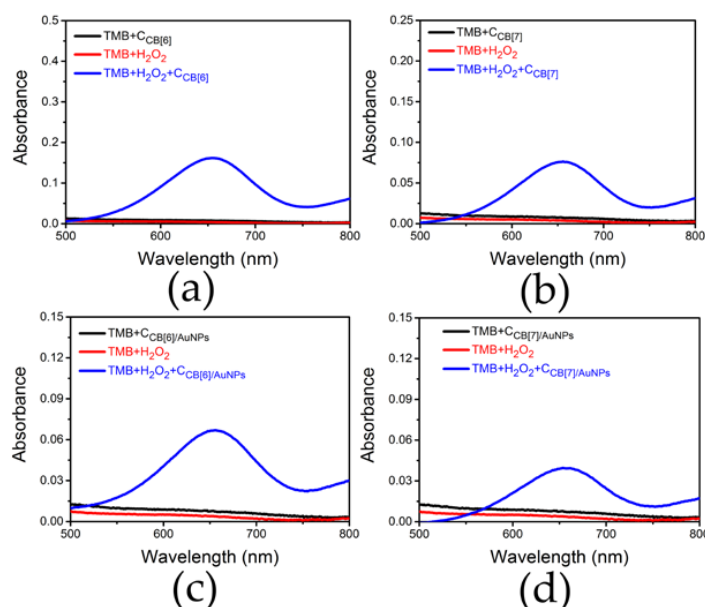


**Figure 4.** UV-vis spectra of different TMB system with (a)  $C_{CB[6]}$ ; (b)  $C_{CB[7]}$ ; (c)  $C_{CB[6]}/AuNPs$ ; (d)  $C_{CB[7]}/AuNPs$ .

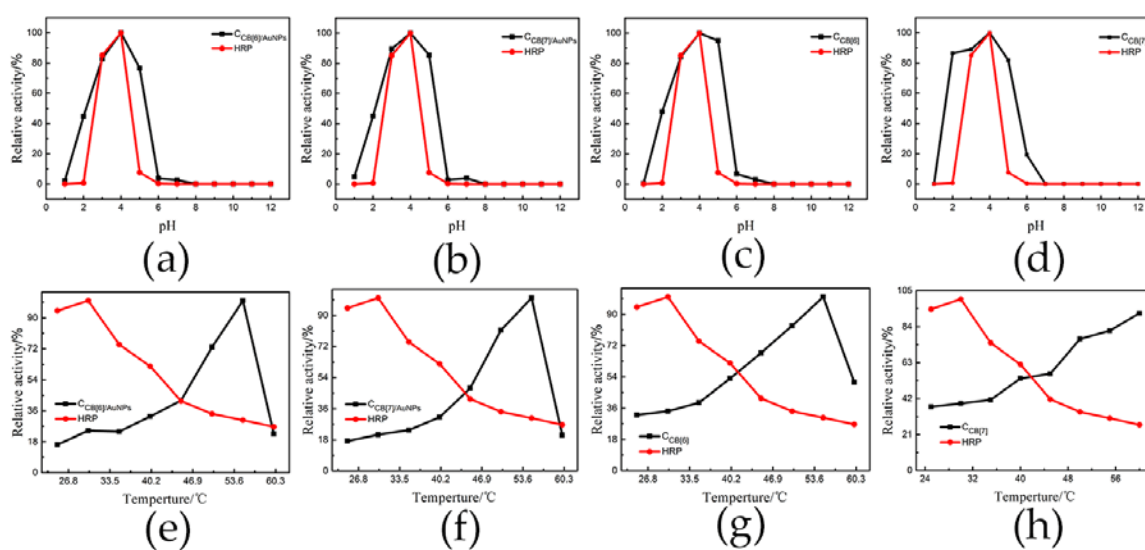


**Figure 5.** pH dependent response curves of different materials in this work and HRP: (a)  $C_{CB[6]}/AuNPs$ ; (b)  $C_{CB[7]}/AuNPs$ ; (c)  $C_{CB[6]}$ ; (d)  $C_{CB[7]}$ . Temperature dependent response curves of different materials in this work and HRP: (e)  $C_{CB[6]}/AuNPs$ ; (f)  $C_{CB[7]}/AuNPs$ ; (g)  $C_{CB[6]}$ ; (h)  $C_{CB[7]}$ .

For further analyzing the catalytic mechanism of hybrids and carbon nanomaterials, steady-state kinetics with TMB and H<sub>2</sub>O<sub>2</sub> as substrates were investigated. A series of experiments were performed by varying the concentration of one substrate while fixing another as constant. Typical Michaelis-Menten curves (Figure 6) were received in a certain concentration of H<sub>2</sub>O<sub>2</sub> or TMB. Maximum initial velocity ( $V_{max}$ ) and Michaelis-Menten constant ( $K_m$ ) were obtained using Lineweaver-Burk plot and were presented in Table 1. Typically, the lower  $K_m$  represents a higher enzyme-like affinity between the catalyst and the substrate [32,35]. The  $K_m$  value of hybrids with TMB was lower than that of carbon nanomaterials and higher than that of CB[n] capped AuNPs (Figure S3). This suggests higher binding affinity of hybrids to TMB than that of carbon nanomaterials, and lower binding affinity of hybrids to TMB than that of CB[n] capped AuNPs. Similarly, the  $K_m$  value of hybrids with H<sub>2</sub>O<sub>2</sub> is slightly lower than that of carbon nanomaterials and higher than that of CB[n] capped AuNPs. The results can be attributed to the synergistic effect of gold and carbon, so hybrids with gold could absorb TMB and H<sub>2</sub>O<sub>2</sub> more efficiently than carbon materials. However, the  $V_{max}$  of carbon nanomaterials is higher than that of hybrids. This is possible as the dispersion of hybrids in water is worse than that of carbon nanomaterials.

Similar to previous studies [36,37], the unsupported CB[n] capped AuNPs could catalyze the oxidation of TMB in the presence of H<sub>2</sub>O<sub>2</sub>. Typically, AuNPs could absorb H<sub>2</sub>O<sub>2</sub> [38] and CB[n] on the gold tend to attract amino groups of TMB electrostatically [3,39], which likely to result in stronger affinity to reaction substrates (Table 1). After carbonization, the unique porous carbon architecture was produced, and the gold was embedded in the porous carbon aggregates, which possibly could benefit electron transfer [40]. Thus far, the hybrids in our case exhibited comparable peroxidase-like activity with Fe<sub>3</sub>O<sub>4</sub>, Pt, Pd and CuS nanoparticles, and much better binding affinity towards H<sub>2</sub>O<sub>2</sub> (Table 1). There is still great potential to improve their ability as nano-enzymes by tuning compositions.

**Table 1.** Michaelis-Menten constant ( $K_m$ ) and maximum reaction rate ( $V_{max}$ ) of different nanomaterials in this work and HRP.

Catalyst	Substrate	$K_m$ (mM)	$V_{max}$ (10 <sup>-9</sup> M/s)
C <sub>CB[6]</sub>	TMB	2.4 ± 0.1	98.2 ± 3.8
	H <sub>2</sub> O <sub>2</sub>	2.2 ± 0.2	16.4 ± 1.8
C <sub>CB[7]</sub>	TMB	2.5 ± 0.1	34.7 ± 2.9
	H <sub>2</sub> O <sub>2</sub>	1.4 ± 0.1	5.2 ± 0.8
CB[6]/AuNPs	TMB	0.098 ± 0.008	10.1 ± 0.8
	H <sub>2</sub> O <sub>2</sub>	0.2 ± 0.07	3.0 ± 0.2
CB[7]/AuNPs	TMB	0.038 ± 0.003	10.2 ± 0.2
	H <sub>2</sub> O <sub>2</sub>	0.097 ± 0.02	3.9 ± 0.1
C <sub>CB[6]</sub> /AuNPs	TMB	1.9 ± 0.2	11.4 ± 1.2
	H <sub>2</sub> O <sub>2</sub>	1.3 ± 0.2	10.8 ± 1.5
C <sub>CB[7]</sub> /AuNPs	TMB	0.63 ± 0.12	6.4 ± 1.0
	H <sub>2</sub> O <sub>2</sub>	0.74 ± 0.08	1.7 ± 1.1
HRP	TMB	0.81 ± 0.11	47.6 ± 2.3
	H <sub>2</sub> O <sub>2</sub>	9.8 ± 0.04	87.6 ± 2.0
Fe <sub>3</sub> O <sub>4</sub> magnetic nanoparticles [30]	TMB	0.098	34.4
	H <sub>2</sub> O <sub>2</sub>	154	97.8
Glutathione-capped Pd nanoparticles [41]	TMB	0.068	315
	H <sub>2</sub> O <sub>2</sub>	156	408
Glutathione-capped Pt nanoparticles [42]	TMB	0.079	328
	H <sub>2</sub> O <sub>2</sub>	73.6	302
Montmorillonite-supported CuS nanoparticles [43]	TMB	0.021	2.8
	H <sub>2</sub> O <sub>2</sub>	2.3	0.97

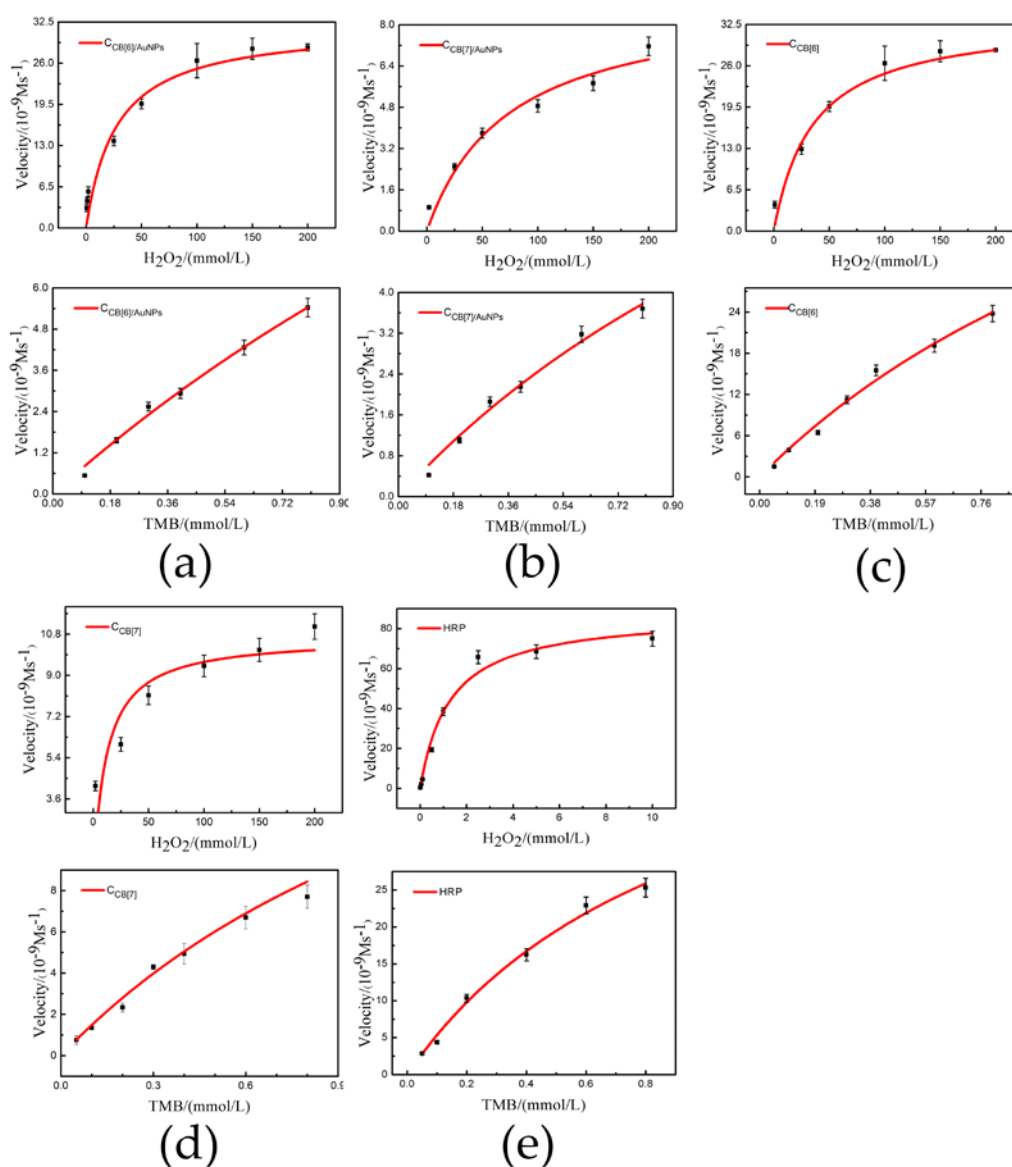


**Figure 6.** Steady-state kinetic curves of different materials in this work and HRP: (a)  $C_{CB[6]}/AuNPs$ ; (b)  $C_{CB[7]}/AuNPs$ ; (c)  $C_{CB[6]}$ ; (d)  $C_{CB[7]}$ ; (e) HRP.

#### 4. Conclusions

In the present work, we prepared well-dispersed AuNPs using cucurbit[*n*]uril ( $n = 6, 7$ ) as reducing and protecting agents according to a facile and eco-friendly one-step synthesis. CB[*n*] based carbon-gold hybrids and carbon nanomaterials were then successfully prepared by carbonization, which is a simple, cost-effective, quick and practical approach. All CB[*n*]based nanomaterials possess intrinsic peroxidase-like activity, and the hybrids could absorb substrates more efficiently with the incorporated gold. This method guided constructing novel and enhanced carbon-gold multifunctional nanomaterials. Once guest molecules containing nitrogen, oxygen and other heteroatoms are included in the cavity of CB[*n*] on metallic nanoparticles, heteroatom-doped carbon-metal hybrids can be prepared.

**Supplementary Materials:** The following are available online at <http://www.mdpi.com/2079-4991/8/5/273/s1>, Figure S1: The time-dependent absorbance changes at 652 nm under different TMB concentration; Figure S2: (a) Temperature and (b) pH dependence for TMB and  $H_2O_2$  system in the absence of nanomaterials; Figure S3:

UV-vis spectra of different TMB system with (a) CB[6]/AuNPs and (b) CB[7]/AuNPs, and steady-state kinetic curves of (c) CB[6]/AuNPs and (d) CB[7]/AuNPs.

**Author Contributions:** S.L. and F.L. conceived and designed the experiments; L.Z. performed the experiments; L.Z., Y.Z. and F.L. analyzed the data; L.Z. and F.L. wrote the paper.

**Acknowledgments:** We acknowledge the financial support from National Natural Science Foundation of China (21372183, 21472143), Thousand Youth Talents Program of China, and Program for Innovative Teams of Outstanding Young and Middle-aged Researchers in the Higher Education Institutions of Hubei Province (T201702).

**Conflicts of Interest:** The authors declare no conflict of interest.

## References

1. Ni, X.L.; Xiao, X.; Cong, H.; Liang, L.L.; Cheng, K.; Cheng, X.J.; Ji, N.N.; Zhu, Q.J.; Xue, S.F.; Tao, Z. Cucurbit[n]uril-based coordination chemistry: From simple coordination complexes to novel poly-dimensional coordination polymers. *Chem. Soc. Rev.* **2013**, *42*, 9480–9508. [[CrossRef](#)] [[PubMed](#)]
2. An, Q.; Li, G.; Tao, C.; Li, Y.; Wu, Y.; Zhang, W. A general and efficient method to form self-assembled cucurbit[n]uril monolayers on gold surfaces. *Chem. Commun.* **2008**, *0*, 1989–1991. [[CrossRef](#)] [[PubMed](#)]
3. Barrow, S.J.; Kasera, S.; Rowland, M.J.; del Barrio, J.; Scherman, O.A. Cucurbituril-Based Molecular Recognition. *Chem. Rev.* **2015**, *115*, 12320–12406. [[CrossRef](#)] [[PubMed](#)]
4. Gurbuz, S.; Idris, M.; Tuncel, D. Cucurbituril-based supramolecular engineered nanostructured materials. *Org. Biomol. Chem.* **2015**, *13*, 330–347. [[CrossRef](#)] [[PubMed](#)]
5. Cui, H.; Hong, C.; Ying, A.; Yang, X.; Ren, S. Ultrathin gold nanowire-functionalized carbon nanotubes for hybrid molecular sensing. *ACS Nano* **2013**, *7*, 7805–7811. [[CrossRef](#)] [[PubMed](#)]
6. Yao, A.; Fu, Q.; Xu, L.; Xu, Y.; Jiang, W.; Wang, D. Synthesis of pH-responsive nanocomposites of gold nanoparticles and graphene oxide and their applications in SERS and catalysis. *RSC Adv.* **2017**, *7*, 56519–56527. [[CrossRef](#)]
7. Khalil, I.; Julkapli, N.M.; Yehye, W.A.; Basirun, W.J.; Bhargava, S.K. Graphene-gold nanoparticles hybrid-synthesis, functionalization, and application in a electrochemical and surface-enhanced raman scattering biosensor. *Materials* **2016**, *9*, 406. [[CrossRef](#)] [[PubMed](#)]
8. Ondera, T.J.; Hamme, A.T. Gold nanopopcorn attached single-walled carbon nanotube hybrid for rapid detection and killing of bacteria. *J. Mater. Chem. B* **2014**, *2*, 7534–7543. [[CrossRef](#)] [[PubMed](#)]
9. Yang, W.; Qu, L.; Zheng, R.; Liu, Z.; Ratinac, K.R.; Shen, L.; Yu, D.; Yang, L.J.; Barrow, C.; Ringer, S.P.; et al. Self-Assembly of gold nanowires along carbon nanotubes for ultrahigh-aspect-ratio hybrids. *Chem. Mater.* **2011**, *23*, 2760–2765. [[CrossRef](#)]
10. Song, J.; Wang, F.; Yang, X.; Ning, B.; Harp, M.G.; Culp, S.H.; Hu, S.; Huang, P.; Nie, L.; Chen, J.; et al. Gold nanoparticle coated carbon nanotube ring with enhanced raman scattering and photothermal conversion property for theranostic applications. *J. Am. Chem. Soc.* **2016**, *138*, 7005–7015. [[CrossRef](#)] [[PubMed](#)]
11. Zhou, X.; Liang, F. Application of graphene/graphene oxide in biomedicine and biotechnology. *Curr. Med. Chem.* **2014**, *21*, 855–869. [[CrossRef](#)] [[PubMed](#)]
12. Liang, F.; Chen, R. Emerging assay platforms based on nanostructures. *Curr. Nanosci.* **2015**, *11*, 684. [[CrossRef](#)]
13. Ma, T.; Liang, F.; Chen, R.; Liu, S.; Zhang, H. Synthesis of Au-Pd bimetallic nanoflowers for catalytic reduction of 4-nitrophenol. *Nanomaterials* **2017**, *7*, 239. [[CrossRef](#)] [[PubMed](#)]
14. Ma, T.; Yang, W.; Liu, S.; Zhang, H.; Liang, F. A comparison reduction of 4-nitrophenol by gold nanospheres and gold nanostars. *Catalysts* **2017**, *7*, 38. [[CrossRef](#)]
15. Shu, T.; Su, L.; Wang, J.; Lu, X.; Liang, F.; Li, C.; Zhang, X. Value of the debris of reduction sculpture: Thiol etching of Au nanoclusters for preparing water-soluble and aggregation-induced emission-active Au(I) complexes as phosphorescent copper ion sensor. *Anal. Chem.* **2016**, *88*, 6071–6077. [[CrossRef](#)] [[PubMed](#)]
16. Lu, X.; Wang, T.; Shu, T.; Qu, X.; Zhang, X.; Liang, F.; Su, L. Combination of chemical etching of gold nanoclusters with aggregation-induced emission for preparation of new phosphors for the development of UV-driven phosphor-converted white light-emitting diodes. *J. Mater. Chem. C* **2016**, *4*, 11482–11487. [[CrossRef](#)]

17. Han, Y.; Yang, X.; Liu, Y.; Ai, Q.; Liu, S.; Sun, C.; Liang, F. Supramolecular controlled cargo release *via* near infrared tunable cucurbit[7]uril-gold nanostars. *Sci. Rep.* **2016**, *6*, 22239. [[CrossRef](#)] [[PubMed](#)]
18. Liu, Y.; Hu, Y.; Chen, R.; Zhan, W.; Ni, H.; Zhang, P.; Liang, F. Antibacterial properties of multi-walled carbon nanotubes decorated with silver nanoparticles. *Curr. Nanosci.* **2016**, *12*, 411–415. [[CrossRef](#)]
19. Liu, Y.; Liu, S.; Chen, R.; Zhan, W.; Ni, H.; Liang, F. An antibacterial nonenzymatic glucose sensor composed of carbon nanotubes decorated with silver nanoparticles. *Electroanalysis* **2015**, *27*, 1138–1143. [[CrossRef](#)]
20. Liu, Y.; Han, Y.; Chen, R.; Zhang, H.; Liu, S.; Liang, F. In situ immobilization of copper nanoparticles on polydopamine coated graphene oxide for H<sub>2</sub>O<sub>2</sub> determination. *PLoS ONE* **2016**, *11*, e0157926.
21. Zhou, Y.; Liu, L.; Shen, Y.; Wu, L.; Yu, L.; Liang, F.; Xi, J. Carbon dots promoted vanadium flow batteries for all-climate energy storage. *Chem. Commun.* **2017**, *53*, 7565–7568. [[CrossRef](#)] [[PubMed](#)]
22. Zeng, Y.; Miao, F.; Zhao, Z.; Zhu, Y.; Liu, T.; Chen, R.; Liu, S.; Lv, Z.; Liang, F. Low-cost nanocarbon-based peroxidases from graphite and carbon fibers. *Appl. Sci.* **2017**, *7*, 924.
23. Liu, Y.; Shen, Y.; Yu, L.; Liu, L.; Liang, F.; Qiu, X.; Xi, J. Holey-engineered electrodes for advanced vanadium flow batteries. *Nano Energy* **2018**, *43*, 55–62. [[CrossRef](#)]
24. Lee, T.C.; Scherman, O.A. A facile synthesis of dynamic supramolecular aggregates of cucurbit[n]uril ( $n = 5–8$ ) capped with gold nanoparticles in aqueous media. *Chem. Eur. J.* **2012**, *18*, 1628–1633. [[CrossRef](#)] [[PubMed](#)]
25. Lee, T.C.; Scherman, O.A. Formation of dynamic aggregates in water by cucurbit[5]uril capped with gold nanoparticles. *Chem. Commun.* **2010**, *46*, 2438–2440. [[CrossRef](#)] [[PubMed](#)]
26. Lanterna, A.; Pino, E.; Domenech-Carbo, A.; Gonzalez-Bejar, M.; Perez-Prieto, J. Enhanced catalytic electrochemical reduction of dissolved oxygen with ultraclean cucurbituril[7]-capped gold nanoparticles. *Nanoscale* **2014**, *6*, 9550–9553. [[CrossRef](#)] [[PubMed](#)]
27. Blanco, E.; Esteve-Adell, I.; Atienzar, P.; Casas, J.A.; Hernández, P.; Quintana, C. Cucurbit[7]uril-stabilized gold nanoparticles as catalysts of the nitro compound reduction reaction. *RSC Adv.* **2016**, *6*, 86309–86315. [[CrossRef](#)]
28. Jose, M.V.; Marx, S.; Murata, H.; Koepsel, R.R.; Russell, A.J. Direct electron transfer in a mediator-free glucose oxidase-based carbon nanotube-coated biosensor. *Carbon* **2012**, *50*, 4010–4020. [[CrossRef](#)]
29. Cui, R.; Liu, C.; Shen, J.; Gao, D.; Zhu, J.-J.; Chen, H.-Y. Gold nanoparticle-colloidal carbon nanosphere hybrid material: Preparation, characterization, and application for an amplified electrochemical immunoassay. *Adv. Funct. Mater.* **2008**, *18*, 2197–2204. [[CrossRef](#)]
30. Gao, L.; Zhuang, J.; Nie, L.; Zhang, J.; Zhang, Y.; Gu, N.; Wang, T.; Feng, J.; Yang, D.; Perrett, S.; et al. Intrinsic peroxidase-like activity of ferromagnetic nanoparticles. *Nat. Nanotechnol.* **2007**, *2*, 577–583. [[CrossRef](#)] [[PubMed](#)]
31. Shi, W.; Wang, Q.; Long, Y.; Cheng, Z.; Chen, S.; Zheng, H.; Huang, Y. Carbon nanodots as peroxidase mimetics and their applications to glucose detection. *Chem. Commun.* **2011**, *47*, 6695–6697. [[CrossRef](#)] [[PubMed](#)]
32. Tao, Y.; Lin, Y.; Huang, Z.; Ren, J.; Qu, X. Incorporating graphene oxide and gold nanoclusters: A synergistic catalyst with surprisingly high peroxidase-like activity over a broad pH range and its application for cancer cell detection. *Adv. Mater.* **2013**, *25*, 2594–2599. [[CrossRef](#)] [[PubMed](#)]
33. Lu, N.; Zhang, M.; Ding, L.; Zheng, J.; Zeng, C.; Wen, Y.; Liu, G.; Aldalbahi, A.; Shi, J.; Song, S.; et al. Yolk-shell nanostructured Fe<sub>3</sub>O<sub>4</sub>@C magnetic nanoparticles with enhanced peroxidase-like activity for label-free colorimetric detection of H<sub>2</sub>O<sub>2</sub> and glucose. *Nanoscale* **2017**, *9*, 4508–4515. [[CrossRef](#)] [[PubMed](#)]
34. Liu, Q.; Yang, Y.; Lv, X.; Ding, Y.; Zhang, Y.; Jing, J.; Xu, C. One-step synthesis of uniform nanoparticles of porphyrinfunctionalized ceria with promising peroxidase mimetics for H<sub>2</sub>O<sub>2</sub> and glucose colorimetric detection. *Sens. Actuators. B Chem.* **2017**, *240*, 726–734. [[CrossRef](#)]
35. Song, Y.; Qu, K.; Zhao, C.; Ren, J.; Qu, X. Graphene oxide: Intrinsic peroxidase catalytic activity and its application to glucose detection. *Adv. Mater.* **2010**, *22*, 2206–2210. [[CrossRef](#)] [[PubMed](#)]
36. Jv, Y.; Li, B.; Cao, R. Positively-charged gold nanoparticles as peroxidase mimic and their application in hydrogen peroxide and glucose detection. *Chem. Commun.* **2010**, *46*, 8017–8019. [[CrossRef](#)] [[PubMed](#)]
37. Wang, S.; Chen, W.; Liu, A.L.; Hong, L.; Deng, H.H.; Lin, X.H. Comparison of the peroxidase-like activity of unmodified, amino-modified, and citrate-capped gold nanoparticles. *ChemPhysChem* **2012**, *13*, 1199–1204. [[CrossRef](#)] [[PubMed](#)]

38. Cui, H.; Zhang, Z.F.; Shi, M.J.; Xu, Y.; Wu, Y.L. Light emission of gold nanoparticles induced by the reaction of bis(2,4,6-trichlorophenyl) oxalate and hydrogen peroxide. *Anal. Chem.* **2005**, *77*, 6402–6406. [[CrossRef](#)] [[PubMed](#)]
39. Yu, F.; Huang, Y.; Cole, A.J.; Yang, V.C. The artificial peroxidase activity of magnetic iron oxide nanoparticles and its application to glucose detection. *Biomaterials* **2009**, *30*, 4716–4722. [[CrossRef](#)] [[PubMed](#)]
40. Zhang, D.; Zhao, H.; Fan, Z.; Li, M.; Du, P.; Liu, C.; Li, Y.; Li, H.; Cao, H. A highly sensitive and selective hydrogen peroxide biosensor based on gold nanoparticles and three-dimensional porous carbonized chicken eggshell membrane. *PLoS ONE* **2015**, *10*, e0130156. [[CrossRef](#)] [[PubMed](#)]
41. Fu, Y.; Zhang, H.; Dai, S.; Zhi, X.; Zhang, J.; Li, W. Glutathione-stabilized palladium nanozyme for colorimetric assay of silver(I) ions. *Analyst* **2015**, *140*, 6676–6683. [[CrossRef](#)] [[PubMed](#)]
42. Li, W.; Zhang, H.; Zhang, J.; Fu, Y. Synthesis and sensing application of glutathione-capped platinum nanoparticles. *Anal. Methods* **2015**, *7*, 4464–4471. [[CrossRef](#)]
43. Zhang, L.; Chen, M.; Jiang, Y.; Chen, M.; Ding, Y.; Liu, Q. A facile preparation of montmorillonite-supported copper sulfide nanocomposites and their application in the detection of H<sub>2</sub>O<sub>2</sub>. *Sens. Actuators B Chem.* **2017**, *239*, 28–35. [[CrossRef](#)]



© 2018 by the authors. Licensee MDPI, Basel, Switzerland. This article is an open access article distributed under the terms and conditions of the Creative Commons Attribution (CC BY) license (<http://creativecommons.org/licenses/by/4.0/>).